MRS Advances © 2018 Materials Research Society
DOI: 10.1557/adv.2018.14

Facile Synthesis of Water-Soluble Graphene Quantum Dots/Graphene for Efficient Photodetector

Sanju Gupta[1], Jared Walden[2], Alexander Banaszak[1] and Sara B. Carrizosa[3]

[1] *Department of Physics and Astronomy and Advanced Materials Institute, Western Kentucky University, Bowling Green, KY 42101, U.S.A.; E-Mail: sanju.gupta@wku.edu*

[2] *Department of Electrical Engineering, Western Kentucky University, Bowling Green, KY 42101, U.S.A.*

[3] *Department of Chemistry, Western Kentucky University, Bowling Green, KY 42101, U.S.A.*

ABSTRACT

Graphene quantum dots (GQDs) are zero-dimensional material with characteristics derived from functionalized graphene precursors are graphene sheets a few nanometers in the lateral dimension having a several-layer thickness. Combining the structure of graphene with the quantum confinement and edge effects, GQDs possess unique chemical behavior and physical properties. Intense research activity in GQDs is attributed to their novel phenomena of charge transport and light absorption and photoluminescence excitation. The optical transitions are known to be available up to 6 eV in GQDs, applicable for ultraviolet photonics and optoelectronics devices, biomedical imaging capabilities and technologies. We present facile hydrothermal and solvothermal methods for synthesizing homogenous dispersed and uniform sized GQDs with a strong greenish and violet blue emission peaks at ~10-14% yield. This approach enabled a large-scale production of aqueous GQD dispersions without the need for chemical stabilizers. The structure and emission mechanism of the GQDs have been studied by combining extensive characterization techniques and rigorous control experiments. We further demonstrate the distinctive advantages of such GQDs as high-performance photodetectors (PDs). Here we also report high-efficient photocurrent (PC) behaviors consisting of multilayer GQDs sandwiched between monolayer graphene sheets. It is conceivable that the observed unique PD characteristics proved to be dominated by tunneling of charge carriers which occurs through the multiple energy states within the bandgap of GQDs, based on bias-dependent variation of the band profiles. This results in novel dark current and PC behaviors. The external quantum efficiency (η) is predicted to be 47% at applied potential 2 V. These findings highlight rich photophysics and comparable performance of graphene/graphene oxide hybrids opening up potential applications as optoelectronic devices.

INTRODUCTION

Carbon-based materials have emerged as attractive candidates in the applications of bio-imaging, catalysis, photovoltaics, and optoelectronic devices because of the advantages of high chemical stability, earthly abundance, and nontoxicity. Graphene, the 2D carbon existing as an atomic thin layer of carbon atoms arranged in a honeycomb lattice, has set the science and technology sectors alight with significant interests in more than a decade [1-7]. It is attributed to their extraordinary physical (electronic, thermal and optical) properties and unique chemical and electrochemical behavior that has wide-ranging potential applications. Despite the excellent properties, monolayer graphene is a zero band gap semimetal that has hindered its applications as semiconductor. There are a few ways to introduce band gap into monolayer graphene and one of the most efficient methods is to constrain graphene edges along two dimensions leading to quantum effects. Alternatively, shrinking the size of graphene sheet until it reduces to zero-dimensional (0D) quantum dots produces graphene quantum dots (GQDs). Intense research interest in GQDs is attributed to their unique physicochemical phenomena arising from the sp2-bonded carbon nanocore surrounded with edged plane functional moieties [8-13]. Moreover, nanostructured materials are attractive for detection applications because they can be integrated with conventional silicon electronics and flexible, large-area substrates, and solution-phase processable using spin casting, spray coating and layer-by-layer deposition. The photonic/ optoelectronic devices and integrated circuits exhibit phenomena including ultraviolet absorption of light, plasmonic enhancement of absorption, size-based spectral tuning, multiexciton generation and charge carrier storage in surface and interface traps [14-16]. In this work, we report on the solution-processed hydrothermal and solvothermal synthesis of stable colloidal and tunable bandgap GQDs from graphene derivatives (graphene oxide; GO and reduced form, rGO). The optimal size less than 10 nm lateral dimension determined using high-resolution transmission electron microscopy, with additional UV-Vis absorption and fluorescence spectroscopy, revealing electronic band signatures in the blue-violet region are presented. A simple GQD-based structure that works as a PD device showing stronger photocurrent in the UV-VIS range is designed and studied. The structure is based on multiple layers of GQDs sandwiched between multiple layers of monolayer graphene sheets. The PD structures are expected to permit large PC flow by tunneling of charge carriers through the energy states in GQDs.

EXPERIMENTAL DETAILS

Materials and methods

GQD synthesis

The hydrothermal and solvothermal techniques have been the most popular and gathering interest from scientists and technologists of different disciplines, particularly in the last two decades [17-19]. We synthesized graphene quantum dots (GQDs) using solvothermal route and hydrothermal method, wherein both GO and rGO as precursors were used (see Ref. [20] for details). Briefly, for solvothermal preparation, 0.5-g GO and 50-mL of N-N dimethylformamide (DMF) produced 10 mg/mL concentrated GO/DMF suspension, ultrasonicated for 1 h, transferred into a 60-mL Teflon-lined stainless steel

autoclave, and heated in a muffle furnace at 140 and 200 °C, for 8 h. The final GQD/DMF product was obtained through vacuum filtration using a 0.2-μm micropore membrane. The GQD/DMF suspension was roto-evaporated to remove DMF and to obtain GQDs, which were then re-dissolved in pure water and phosphate-buffered saline (PBS) to produce different suspensions. The GO/DMF of 0.5, 1, 5, 10, and 20 mg/mL were strictly controlled with 40%, 60%, and 80% ratios and reaction times of 8h and 12h. To select the optimal preparation conditions, the fluorescence quantum yield of different GOD samples was measured using fluorescence spectroscopy (excitation wavelength of 420 nm) with DMF as reference. For hydrothermal method, GO nanosheet was partially deoxidized in a tube furnace at < 300 °C for 2h in Ar atmosphere. The thermally reduced GO nanosheet dispersions of 1.0 mg/mL in deionized (DI) water was prepared by stirring 8h and mild ultrasonication for approximately 40 min. These dispersions were purified with microporous (0.2 μm) polytetrafluoroethylene (PTFE) membrane and re-dispersed in DI water. Then the suspensions were heated at 200 °C, 170 °C and 140 °C for 8-10h in a Teflon-lined stainless steel autoclave. The resulting black suspensions were filtered with PTFE membrane and a dark brown filtered solution was obtained. To remove larger graphene nanoparticles, the colloidal solution was dialyzed retaining molecular weight, 3500 Da overnight. The GQDs obtained from these two precursors showed stability over six months. These dispersions were drop cast followed by air drying on commercial substrates and to prepare device under test as needed for various characterization mentioned below.

Structural and optical properties and device characterization

The GQD samples were characterized to obtain average crystal and lattice structure, optical absorption and photoluminescence spectra and photodetection properties. Samples for high-resolution transmission electron microscopy (HR-TEM) were prepared by placing two drops of GQDs on commercial Cu grids coated with lacey carbon (Ted Pella Inc., Redding, CA, USA) and allowing to air dry. They were taken using a JEOL instrument (Model 1400 Plus, OR, Peabody, MA, USA) operating at 200 kV and 1 nA. TEM measurements provided size distribution, intrinsic microstructure and lattice spacing. The EDX (Energy Dispersive Spectroscopy) signals were measured using an EDX detector yielding C/O ratio of 8:1 for both GQDs prepared using GO and rGO. Interestingly, GO is partially reduced while undergoing hydrothermal treatment. X-ray diffraction (XRD) patterns were obtained with Siemens Model D5000 instrument (Thermo Scientific, MA) in Bragg-Brentano θ-2θ geometry ranging 2θ from 8° to 30° using Cu K_α X-ray source (λ=1.5405 Å) operating at voltage of 45 kV and current 40 mA. Samples were run at a scan rate of 0.04 °/s or to improve scattering signal counts, we measured at 0.02°/s scan rate. The optical (UV-Vis absorption and fluorescence) spectroscopy measurements were taken using a BioTek spectrometer (Model Synergy H1 Multi-mode Reader, Winooski, VT, USA) equipped with a xenon lamp as broadband excitation source. For fluorescence measurements, the excitation wavelength λ_{ex} = 370 nm and spectral window of 350–550 nm was used with wavelength interval 0.5 nm and for UV-Vis the absorption spectroscopy is measured between 210 and 550 nm in interval of 1 nm. All the measurements were carried out at room temperature (~298K). Raman spectroscopy was carried out to determine the lattice vibration structure at various points on GQDs and other samples. The Raman spectra were recorded using a micro-Raman spectrometer (Model InVia Renishaw plc, Gloucestershire, UK) equipped with laser excitation wavelength 633 nm (E_L=1.92 eV) and ~1 mW power incident at the sample, with edge filters cutting at ~100 cm^{-1} and an objective lens of 50× providing spot size ~2 μm. The scattered light from the sample is collected in backscattering geometry,

transmitted by a beam splitter, and detected by a CCD camera. Extreme care was taken to avoid sample damage caused by laser-induced thermal degradation and therefore 1 or 5% light intensity was used to obtain spectra for 60-300s to optimize the signal-to-noise ratio. Raman shift ranged from 1100 to 3200 cm^{-1} with a spectral resolution of 1 cm^{-1}. To prepare the photodetector devices (see Figure 1, panels a and b), the monolayer graphene/SiO_2/p-Si stack were used as starting layer and annealed at 400 ^oC for 1h in vacuum to remove the surface adsorbates. A 500 µl solution of GQDs was then dropped and spin-coated on the 10x10 mm^2 graphene/SiO_2/p- Si wafer, and annealed at 100 oC for 1 min. This process was repeated at least 5 times to enhance the density of GQDs. Subsequently, a 5 x 5 mm^2 single-layer graphene was coated on 1/3 area of the GQDs/graphene/SiO_2/p-Si wafer, and annealed at 400 ^oC for 1 h in vacuum. As a result, the graphene/GQDs/graphene sandwich structure was formed. Au electrodes of 1-2 mm diameter and 1 mm thickness were deposited on the top of both graphene sheets by thermal evaporation to complete the GQD PD sandwich device. The junction between Au and graphene is expected to be ohmic based on previous reports. For planar or field-effect transistor type device configuration, we prepared two planar electrodes as shown

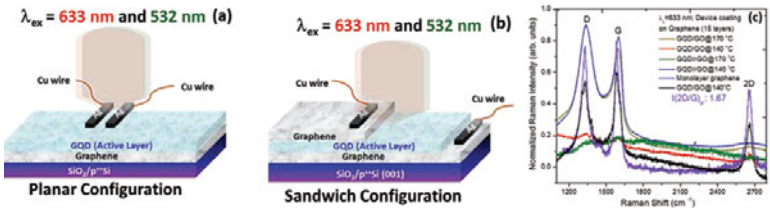

Figure 1. (a, b) GQD PD device architectures used in this study and (c) Raman spectra at of coating layers while fabricating devices showing characteristic bands associated with graphene and GQD.

in Figure 1 (panel a), separated by 1-2 mm exposing GQD as active layer while graphene was underneath coated on SiO_2/p-Si wafer. Figure 1 (panel c) also shows Raman spectra of each of the graphene and GQD layers as device fabrication process is progressed. The result shows that no structural alterations of GQDs occur during the GQD PD fabrication. For device property measurements, we used a custom-designed electrical property measurement set-up with LabView software integrated with Raman microscope equipped with two lasers of different excitation wavelengths i.e. 633 nm and 532 nm.

RESULTS AND DISCUSSION

Microscopic structural characterization

Figure 2 presents representative transmission electron microscopy images of hydrothermally prepared GQDs from GO revealing the surface morphology, monodispersity and average particle size (~5–7 nm) of the GQDs with interplanar spacing, d002 ~0.537 nm (ca. parent graphite, 0.34 nm); the latter is derived from the presence of Moiré fringes. Under hydrothermal conditions of lower temperature and pressure in autoclave, partial reduction of GO into rGO occurs. Structural order is evident from the lattice fringe patterns associated with crystalline graphene sheets. The crystalline structure of GQDs is investigated by X-ray diffraction (XRD) and micro-

Raman spectroscopy (RS) shown in Figure 2 (panels a and b). The GQDs contain similar types of oxygenated functional groups as their precursors, including carbonyl (-C=O), carboxyl (-COOH), epoxy (-O-), and hydroxyl (-OH), distributed at the multilayered terrace or edge planes and preferential reduction produces reduced GQDs. The energy-dispersive X-ray spectroscopy (EDX) spectra (not shown) yielded C to O ratios ranging between 55.34 and 69.27 at. %, as anticipated. The interlayer distance of GQDs calculated from the XRD peaks position at $2\theta=12.9^{o}$ and 14.3^{o} assigned to (002) atomic plane correspond to d_1= 0.685 nm and d_2= 0.619 nm [21-22]. The micro-Raman spectra are displayed in Figure 1d prepared with GO at 140, 170 and 200 °C. For a realistic comparison, the spectra are normalized to G band. Raman spectra show prominent signatures correspond to the defects-mediated D band (~1350 cm^{-1}) in the graphene basal plane and characteristic peak associated with in-plane C-C stretching G band in Csp^2 materials occurring at ~1590 cm^{-1}. It is worth mentioning that no evidence about the disorder-induced signal (D' band) occurring at 1620 cm^{-1} has been offered. The intensity ratio of D to G band (I_D/I_G) is a semi-quantitative measure of structural order, i.e. in-plane Csp^2 clustering, larger ratio mean smaller Csp^2 nanodomains. Raman spectra show relatively lower level of defect (ID/IG <0.6) [Figure 2]. UV-Vis absorption and photoluminescence peaks at 440 (2.81 eV) and 650 nm (1.90 eV), excited at 532 nm and 340 nm, respectively, are characteristic of apparently red and blue GQDs according to various reports.20 The absorption band at ~270 nm corresponds to π(bonding)−π* (antibonding) transition (characteristic of natural π-conjugated graphene sheets) of aromatic Csp^2 domains. Like most of the work reported, as-synthesized GQDs possess excitation wavelength-dependent PL (PLE), where the spectral maxima shift with excitation energy [20]. It is proposed that the blue shift of PL maxima is due to quantum confinement of excitons, according to which the smaller the GQDs size, the wider the bandgap and the higher the emission energy. Moreover, the oxygenated functional groups combined with atomic scale defects produce irregularly hybridized π states, which induces energy states in-between the HOMO/LUMO gap that serve as intermediate or mid-gap states between bonding and anti-bonding states. All the microscopic structural characterization indicates that high crystalline quality GQDs are synthesized successfully.

GQD-based photodetector device under test characterization

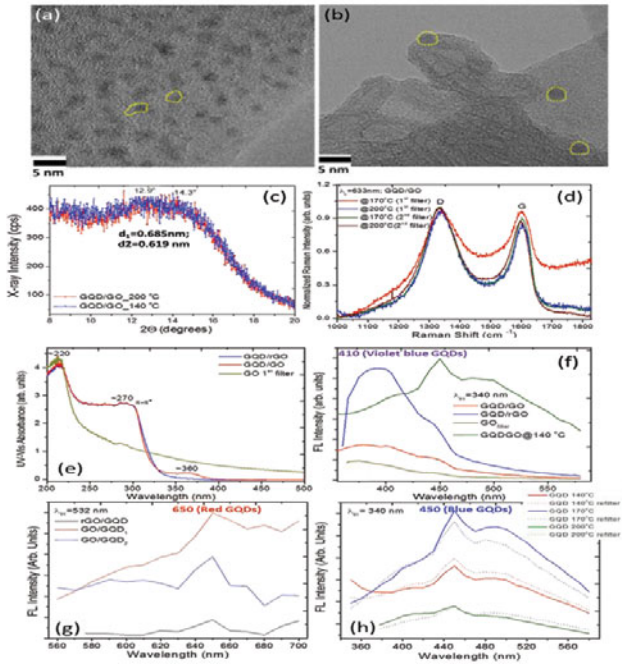

Figure 2. (a, b) TEM micrographs showing both GQD and GO nanosheets, (c) X-ray diffractograms and (d) Raman spectra of GQDs prepared from GO at various synthesis temperatures, (e) UV-Vis absorption spectra, (f-h) room temperature photoluminescence spectra excited at different wavelengths showing blue and green GQDs emission with weaker red emission.

Figure 3 shows dark and photocurrent I-V properties at two different laser wavelengths and for two configurations of device. The positive voltage was applied to Au electrode on upper graphene layer with respect to Au electrode on lower graphene layer/SiO_2 under forward bias. The graphene on graphene junction without GQD under dark and illuminated conditions as control device showed symmetric and linear in forward and reverse bias thus indicating no tunnel behavior (not shown). In contrast, the dark I-V curve of GQD device exhibited somewhat asymmetric and nonlinear behavior with bias voltage, typical of tunneling diodes. These I-V characteristics can be attributed to tunneling at room temperature through the available density of states within the bandgap of GQDs sandwiched between the metallic graphene sheets and biased graphene/GQDs/graphene device. We believe that total measured total current (DC +photocurrent, PC) becomes larger for certain illumination power and for V>0, and PC exceeds DC by almost one order of magnitude. However, the total current for V <0 increases marginally as compared with DC current. Due to multiple scattering of light between GQDs and top graphene the maximum absorption of light takes place in GQDs. Absorption of photons in the GQDs produce electron-hole pairs and for V >0 both electrons and holes photoexcited in the GQDs contribute to the total current. In graphene, the relaxation due to carrier-phonon scattering is much slower than due to carrier-carrier scattering, a single photon can produce multiple electron-hole excitations by impact ionization induced by a hot electron. For V<0 photoexcited electrons in GQD transport to bottom graphene and the higher potential barrier between GQD and bottom graphene

reduced PC (see Fig. 3a-3c). The current from photoexcited holes is limited due to the higher potential barrier between GQDs and top graphene for holes. Thus, for reverse bias ($V < 0$) the total current is almost unaffected by photon absorption. The observed slight enhancement and asymmetry in the total current under illumination can be understood from carrier multiplication. At high enough voltages the total I-V curves are symmetric because the kinetic energy of carriers exceeds the potential barriers on both sides and hence, the tunneling current is not affected by the barriers. These I-V characteristics under dark as well as under illumination were almost unvaried by using Ag as electrode (not shown). The photoresponse (or responsivity, R=Ipc/Popt) typically depend on the excitation photon wavelength. The Figure 3d shows the spectral response with voltage for two different wavelengths used in this study. There are no obvious peaks or valleys

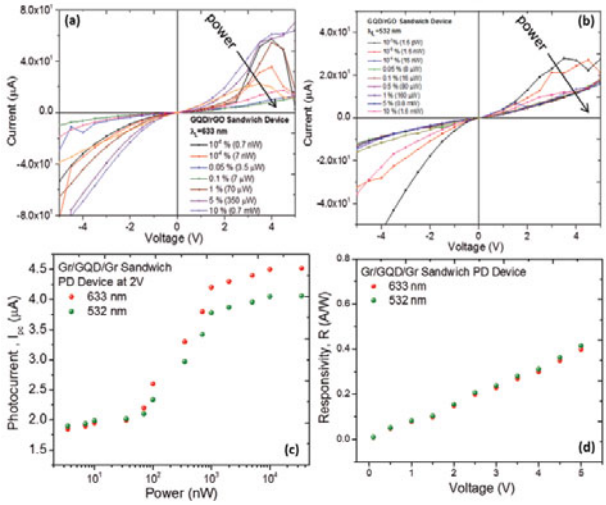

Figure 3. (a, b) Dark and photo I-V characteristics and bias-dependent properties at photon wavelength 633 nm, (c) photocurrent with power, and (d) responsivity with forward bias at room temperature at 633 and 532 nm wavelengths.

in responsivity behavior and it is known that the strong enhancement and quantum efficiency (~ 0.47 or 47% at 2 V) is in the high energy of photons in the visible range.

CONCLUSIONS

Overall, this study successfully prepared GQDs from functionalized graphene derivatives such as GO using a facile water-soluble hydrothermal synthesis approach. This method allowed creating tunable bandgap graphene quantum dots preferentially fluorescence in blue emission for those processed at temperatures of 170 oC and 140 oC, with a smaller yield fraction of red GQDs, for photonic and biomedical imaging applications. We performed systematic structural characterization using complementary

analytical tools to identify the lateral size of GQDs (5-7nm) and crystalline quality. The room temperature electrical property (I-V) measurements in dark and under illumination displayed apparent semiconducting behavior for all of the samples. The photo I-V properties of graphene/GQDs/graphene PD revealed higher responsivity and quantum efficiency. The achievement of high-performance GQD PDs at room temperature suggests that GQDs can be employed for transparent and foldable optoelectronic devices that may open exciting opportunities not only for the creation of single-function PDs in detecting optical signals in wide spectral range but also for the fabrication of key component in biomedical imaging, remote sensing, optical communication and optoelectronic integrated circuits (OEI

ACKNOWLEDGMENTS

The authors (S.G., J.W., A.B. R. M.) gratefully acknowledge financial support in parts from KY NSF REG, KY NSF RSP, KY NASA RIDG, KSEF-RDE and NSF KY EPSCoR RSP Grants and WKU Research Foundation RCAP-I Award. The authors (J.W. and S.B.C.) thank Dr. J. Andersland, Biology for SEM and Ms P. Norris, AMI for XRD training.

REFERENCES

1. A. Geim and K. Novoselov, Nature Mater. 6, 183 (2007).
2. S. Gupta and S. B. Carrizosa, J. Electron. Materials 44, 4492 (2015).
3. S. Gupta, M. vanMeveren and J. Jasinski, Int. J. Electrochem. Sci. 10, 10272 (2015).
4. S. Bai, K. Zhang, L. Wang, J. Sun, R. Luo, D. Li and A. Chen, J. Mater. Chem. A 2, 7927 (2014).
5. G. Wang L. Zhang and J. Zhang, Chem. Soc. Rev. 41, 797 (2012).
6. A. Geim and K. S. Novoselov, Nat. Mater. 6, 652 (2007).
7. R. Raccichini, A. Varzi, S. Passerini and B. Scrosati, Nat. Mater. 14, 271 (2015).
8. Q. Zhang, J. Jie, S. Diao, Z. Shao, Q. Zhang, L. Wang, W. Deng, W. Hu, H. Xia, X. Yuan and S.-T. Lee, ACS Nano 9, 1561 (2015).
9. G. Konstantatos, M. Badioli, L. Gaudreau, J. Osmond, M. Bernechea, F. Pelayo G. de Arquer, F. Gatti and F. H. L. Koppens, Nat. Nanotechnol. 7, 363 (2012).
10. Y. Li, Y. Hu, Y. Zhao, G. Shi, L. Deng, Y. Hou and L. Qu, Adv. Mater. 23, 776 (2011).
11. X. Yan, X. Cui and L. S. Li, J. Am. Chem. Soc. 132, 5944 (2010).
12. G. Konstantatos and E. H. Sargent, Nat. Nanotechnol. 5, 391 (2010).
13. Y. Sun, S. Wang, C. Li, P. Luo, L. Tao, Y. Wei and G. Shi, Phys. Chem. Chem. Phys. 15, 9907 (2013).
14. L. E. Brus, Appl. Phys. 53, 465 (1991).
15. A. L. Efros and M. Rosen, Ann. Rev. Mater. Sci. 30, 475 (2000).
16. C. O. Kim, S. W. Hwang, S. Kim, D. H. Shin, S. S. Kang, J. M. Kim, C. W. Jang, J. H. Kim, K. W. Lee, S.-H. Choi and E. Hwang, Sci. Rep. 4: 5603 (2014).
17. K. Byrappa, M. Yoshimura, in Handbook of Hydrothermal Technology (Noyes Publications, New Jersey, USA, 2001).
18. R. Roy, J. Sol. Stat. Chem. 111, s11–17 (1994).
19. G. Eda and M. Chowalla, Adv. Mater. 22, 2392 (2010).
20. D. Pan, J. Zhang, Z. Li and M. Wu, Adv. Mater. 22, 734 (2010).
21. S. Gupta, T. Smith, A. Banaszak and J. Boeckl, Nanomaterials 7, 301 (2017).
22. C. Xiong, A.E. Aliev, B. Gnade and K.J. Balkus Jr. ACS Nano 2, 293 (2008).
23. E. H. Lee, M. B. Lewis, P. J. Blau, and L. K. Mansur, J. Mater. Res. 6, 610 (1991).